Int. J. Solids Structures Vol. 30, No. 7, pp. 899–919, 1993
Printed in Great Britain

0020–7683/93 $6.00+ .00

MODE I CRACK PROPAGATION IN ELASTIC–PLASTIC PRESSURE-SENSITIVE MATERIALS

DAVIDE BIGONI and ENRICO RADI
Istituto di Scienza delle Costruzioni, Facoltà di Ingegneria, Università di Bologna, Viale Risorgimento, 40136 Bologna, Italy

(*Received* 10 *March* 1992; *in revised form* 28 *September* 1992)

Abstract—Mode I steady-state, quasi-static crack propagation is analysed for elastoplastic pressure-sensitive solids. In particular, reference is made to the incremental small strain elastoplasticity obeying the Drucker–Prager yield condition with associative flow law. The asymptotic crack-tip fields are numerically obtained for the case of linear-isotropic hardening, under plane stress and plane strain conditions.

1. INTRODUCTION

The problem of the determination of asymptotic stress and strain fields in the plastic zone near a crack tip for elastoplastic materials under mode I conditions has been extensively analysed. In particular, the case of quasi-static growth for ideal plasticity was analysed by Slepyan (1974), Gao (1987), Rice *et al.* (1980), Drugan *et al.* (1982) and Rice (1982). The case of J_2-flow theory with linear hardening was first studied by Amazigo and Hutchinson (1977) on the basis of previous works on the singularity ahead of a stationary crack for J_2-deformation theory of plasticity (Hutchinson, 1968a,b; Rice and Rosengren, 1968). The problem was further developed by considering plastic reloading on crack flanks by Ponte Castañeda (1987a). Finally Achenbach *et al.* (1981) and Östlund and Gudmundson (1988) considered dynamic propagation.

In pressure-sensitive materials, the yield locus is dependent on the mean normal stress. Therefore the J_2-flow theory becomes inadequate. The yield surface proposed by Drucker and Prager (1952) is a modification of the Huber–von Mises criterion, represented by a cone in the Haigh–Westergaard stress space. This criterion may be appropriate for the description of the behavior of various materials. In fact, for porous metals (Needleman and Rice, 1978), metals showing the Strength Differential (S-D) effect (Drucker, 1973; Gupta, 1977; Spitzig *et al.*, 1975, 1976), plastics (Carapellucci and Yee, 1986; Spitzig and Richmond, 1979; Whitney and Andrews, 1967), ceramics (Chen and Reyes-Morel, 1986; Reyes-Morel and Chen, 1988), concrete (Kotsovos and Newman, 1978), soils and rocks (Evans and Wong, 1985; Rudnicki, 1977), the Drucker–Prager yield criterion is suitable in the modeling of the appearance of inelastic deformations. When used in connection with the associative flow-rule, the Drucker–Prager yield function predicts a plastic volumetric dilatancy, that generally is an overestimation of the dilatancy observed in the experiments. In fact, the experimental results on high strength steels showing the S-D effect of Spitzig *et al.* (1976) show a dilatancy 15 times inferior to that predicted by the associative law. The experimentally observed dilatancy becomes six times inferior in the case of polyethylene (Spitzig and Richmond, 1979), and, finally, in zirconia-containing ceramics the dilatancy fits coherently with the predictions of the associative flow-rule (Reyes-Morel and Chen, 1988). It is to be observed, however, that the dilatancy measurements are generally averaged over a finite zone and thus such global measure of dilatancy can underestimate the dilatancy in a fracture process zone. Therefore, an asymptotic determination of near-tip stress and strain fields for an elastoplastic model, based on the Drucker–Prager yield surface with associative flow-rule, may be useful for the understanding of fracture in ceramics, amorphous rocks at low temperature, plastics and metals showing the S-D effect. For ductile pressure-sensitive materials, like porous and void nucleating metals, numerous F.E. simulations [see, e.g. Aoki *et al.* (1984, 1987), Needleman and Tvergaard (1987, 1992)] have been performed for static and dynamic crack problems, using the Gurson (1977) model. It

is to be mentioned that these models are in essence similar to a Drucker–Prager model with non-associative flow-rule in which the yield surface gradient and the flow-mode tensor change their direction in the stress space during plastic deformation.

Li and Pan (1990a,b) and Li (1992) studied the asymptotic fields of a stationary crack for ideal plasticity and for deformation theory adopting Drucker–Prager yield surface with associative flow-rule. As is well-known, the deformation theory of plasticity can be considered a good approximation of the real elastoplastic behavior only under peculiar conditions (Budiansky, 1959). Therefore, except for the statical problem, i.e. in the case of crack propagation, the appearance of elastic sectors in the solution [see, e.g. Amazigo and Hutchinson (1977)] makes the results of deformation theory questionable.

The present paper is addressed to the study of mode I steady-state crack propagation in elastoplastic solids with the Drucker–Prager yield condition and linear-isotropic hardening. Numerical results are given for the amplitude of the plastic sector, for the order of the stress singularity and for the near tip stress and velocity fields. The results are obtained for various values of the hardening parameter and of the pressure-sensitivity parameter μ, with a procedure similar to that of Ponte Castañeda (1987a).

Under conditions of plane stress, in connection with the increase in the pressure-sensitivity, a substantial decrease is observed in the ratio between the radial and the hoop stresses ahead of the crack tip. In particular, for low values of hardening, the mentioned ratio tends to zero when μ approaches a definite value between 0.8 and 0.9. Moreover, a decrease is observed in the opening stress and in the mean stress directly ahead of the tip in relation to the increase of the pressure-sensitivity. Further, the size of the plastic sector ahead of the tip decreases by increasing the pressure-sensitivity. These circumstances are in good agreement with the results of Li and Pan (1990b) and Li (1992) for a stationary crack in the elastic–perfectly plastic theory.

Under conditions of plane strain, the pressure-sensitivity relaxes the stress deviator ahead of the crack tip. This result is coherent with those of Li and Pan (1990a) and, for a different pressure-sensitive model, of Hutchinson (1982). Moreover, analogously to the case of plane stress, the singularity of the fields becomes weaker by increasing the pressure-sensitivity. The pressure-sensitivity of the model adopted leaves open the possibility of taking the effect of the non-associativity of the flow-rule into account. This possibility is systematically explored elsewhere (Radi and Bigoni, 1992), in the case of plane stress.

2. BASIC RELATIONSHIPS

Constitutive equations

Reference is made to an isotropic elastoplastic model with linear hardening based on the Drucker–Prager (1952) yield function:

$$f(\boldsymbol{\sigma}) = \frac{\mu}{3}\operatorname{tr}\boldsymbol{\sigma} + \sqrt{J_2} - \ell, \tag{1}$$

where $\boldsymbol{\sigma}$ denotes the stress tensor, J_2 the second invariant of deviatoric stress, the hardening parameter ℓ is $1/\sqrt{2}$ times the radius of the section of the yield surface with the π-plane in the Haigh–Westergaard stress space and μ is the measure of the pressure-sensitivity. In particular, μ is related to the flow strengths in tension f_t and compression f_c by the relation:

$$\mu = \sqrt{3}\frac{f_c - f_t}{f_c + f_t}. \tag{2}$$

The elastoplastic stress–strain relationships relating the stress rate $\dot{\boldsymbol{\sigma}}$ to the velocity of deformation $\dot{\boldsymbol{\varepsilon}}$ can be deduced, via Prager consistency, to the form:

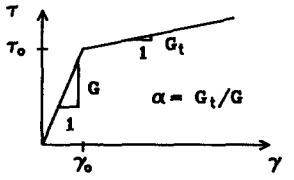

Fig. 1. Stress–(engineering)strain relation in shear.

$$\dot{\varepsilon} = \frac{1}{E}\left[(1+\nu)\dot{\sigma} - \nu(\operatorname{tr}\dot{\sigma})\mathbf{I} + \frac{1}{\hbar}\langle \mathbf{Q}\cdot\dot{\sigma}\rangle \mathbf{Q}\right], \tag{3}$$

where ν is the Poisson ratio, E the elastic modulus, $\hbar$ the hardening modulus divided by E, the symbol $\langle\ \rangle$ denotes the McAulay brackets, i.e. the operator $\langle\gamma\rangle = (\gamma + |\gamma|)/2$ $(\forall\,\gamma \in \mathbb{R})$, and $\mathbf{Q}$ is the gradient of the yield function (1):

$$\mathbf{Q} = \frac{\mu}{3}\mathbf{I} + \frac{\mathbf{S}}{2\sqrt{J_2}}, \tag{4}$$

where $\mathbf{S}$ is the deviatoric stress. As is well known, eqn (3) holds only if the stress point lies on the yield surface, i.e. if $f = 0$.

It is to be remarked that the model reduces to the J_2 elastoplasticity, when the parameter μ is set equal to zero.

Finally, it should be noted that the hardening modulus is related to the ratio α between the tangent modulus G_t and the elastic shear modulus (Fig. 1) and to the ratio χ between the uniaxial tangent modulus and the elastic modulus, through the equations:

$$\alpha^{-1} = 1 + \frac{1}{2(1+\nu)\hbar}, \quad \chi^{-1} = 1 + \frac{1}{\hbar}\left(\frac{\mu}{3} \pm \frac{1}{\sqrt{3}}\right)^2, \tag{5}$$

where the positive sign in (5_2) refers to uniaxial tension and the negative to uniaxial compression. In the case $\mu = 0$ and $\nu = 1/2$, eqns (5) yield $\alpha = \chi$.

Kinematic conditions

A Cartesian reference system is employed, as indicated in Fig. 2, with the origin attached to the moving crack tip. The x_1-axis is oriented in the direction of the crack advance and the x_3-axis coincides with the direction of zero stress (strain) in plane stress (strain). For this choice of the reference frame, the steady-state propagation condition implies that any material derivative can be identified with a spatial derivative in the direction x_1, i.e.

$$(\dot{}) = -\mathscr{V}(\ )_{,1}, \tag{6}$$

where $\mathscr{V}$ denotes the (constant) crack-tip speed and comma indicates differentiation.

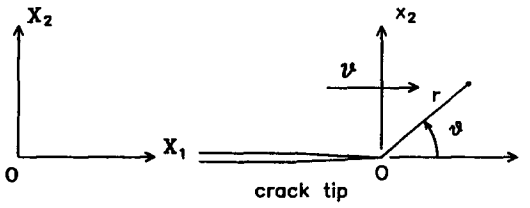

Fig. 2. Frame of references on the crack tip.

However, eqn (6) can be considered well approximated even for non-constant tip speed, when $r \to 0$ (Östlund and Gudmundson, 1988).

The plane stress (strain) problem presents five (six) unknowns, i.e. the non-zero stress components and the two in-plane velocities v_1, v_2, related to the velocity of deformation through the compatibility condition

$$\dot{\varepsilon} = \tfrac{1}{2}[\nabla \mathbf{v} + (\nabla \mathbf{v})^{\mathrm{T}}]. \tag{7}$$

Equations (3), together with the equilibrium equations, allow us to solve the problem of near crack-tip field determination.

Equilibrium equations

For algebraic convenience, a cylindrical coordinate system (r, ϑ, x_3) is introduced. Symmetry of the mode I problem restricts the analysis to the interval $0 \leqslant \vartheta \leqslant \pi$. The equilibrium equations (under plane conditions) in cylindrical coordinates are written as:

$$\begin{aligned} &(r\sigma_{rr})_{,r} + \sigma_{r\vartheta,\vartheta} - \sigma_{\vartheta\vartheta} = 0, \\ &(r\sigma_{r\vartheta})_{,r} + \sigma_{\vartheta\vartheta,\vartheta} + \sigma_{r\vartheta} = 0. \end{aligned} \tag{8}$$

Form of solution

By using (6) and taking into account the transformation rule of differentiation, between Cartesian and polar coordinates:

$$\begin{aligned} (\ )_{,1} &= \cos\vartheta\,(\ )_{,r} - \frac{\sin\vartheta}{r}(\ )_{,\vartheta}, \\ (\ )_{,2} &= \sin\vartheta\,(\ )_{,r} + \frac{\cos\vartheta}{r}(\ )_{,\vartheta}, \end{aligned} \tag{9}$$

the following expressions of the components of the stress rate tensor in cylindrical coordinates are obtained (see Appendix):

$$\begin{aligned} \dot{\sigma}_{r\vartheta} &= \mathscr{V}\left[\frac{\sin\vartheta}{r}\sigma_{r\vartheta,\vartheta} - \cos\vartheta\,\sigma_{r\vartheta,r} + \frac{1}{r}\sin\vartheta\,(\sigma_{rr} - \sigma_{\vartheta\vartheta})\right], \\ \dot{\sigma}_{rr} &= \mathscr{V}\left(\frac{\sin\vartheta}{r}\sigma_{rr,\vartheta} - \cos\vartheta\,\sigma_{rr,r} - \frac{2}{r}\sin\vartheta\,\sigma_{r\vartheta}\right), \\ \dot{\sigma}_{\vartheta\vartheta} &= \mathscr{V}\left(\frac{\sin\vartheta}{r}\sigma_{\vartheta\vartheta,\vartheta} - \cos\vartheta\,\sigma_{\vartheta\vartheta,r} + \frac{2}{r}\sin\vartheta\,\sigma_{r\vartheta}\right), \\ \dot{\sigma}_{33} &= \begin{cases} 0 & \text{(plane stress)}, \\ \mathscr{V}\left(\dfrac{\sin\vartheta}{r}\sigma_{33,\vartheta} - \cos\vartheta\,\sigma_{33,r}\right) & \text{(plane strain)}. \end{cases} \end{aligned} \tag{10}$$

Moreover, in cylindrical coordinates, (7) becomes:

$$\begin{aligned} \dot{\varepsilon}_{rr} &= v_{r,r}, \\ \dot{\varepsilon}_{\vartheta\vartheta} &= \frac{1}{r}(v_{\vartheta,\vartheta} + v_r), \\ \dot{\varepsilon}_{r\vartheta} &= \frac{1}{2}\left[v_{\vartheta,r} + \frac{1}{r}(v_{r,\vartheta} - v_\vartheta)\right], \end{aligned}$$

$$\dot{\varepsilon}_{33} = \begin{cases} v_{3,3} & \text{(plane stress)}, \\ 0 & \text{(plane strain)}. \end{cases} \tag{11}$$

It is worth noting that the equilibrium equations (8) and the constitutive relations (3) are homogeneous in r and, therefore, solutions are sought [e.g. Amazigo and Hutchinson (1977) and Ponte Castañeda (1987)] in a separable form, similar to the HRR fields (Hutchinson, 1968a,b; Rice and Rosengren, 1968):

$$\begin{aligned} v_r(r,\vartheta) &= \mathscr{V}\underline{r}^s \frac{1}{s} y_1(\vartheta), \\ v_\vartheta(r,\vartheta) &= \mathscr{V}\underline{r}^s \frac{1}{s} y_2(\vartheta), \\ \sigma_{r\vartheta}(r,\vartheta) &= E\underline{r}^s y_3(\vartheta), \\ \sigma_{rr}(r,\vartheta) &= E\underline{r}^s y_4(\vartheta), \\ \sigma_{\vartheta\vartheta}(r,\vartheta) &= E\underline{r}^s y_5(\vartheta), \\ \sigma_{33}(r,\vartheta) &= \begin{cases} 0 & \text{(plane stress)}, \\ E\underline{r}^s y_6(\vartheta) & \text{(plane strain)}, \end{cases} \end{aligned} \tag{12}$$

where s is the stress singularity coefficient and the r subscript bar denotes that this variable is non-dimensionalized with respect to any characteristic dimension of the plastic zone. The indetermination in the choice of the non-dimensionalization reflects the well-known circumstance (Ponte Castañeda, 1987b) that the stress solution will be known except for an amplitude factor.

Unloading condition

The generic particle ahead of the crack tip, moving towards the tip, experiences unloading when the plastic multiplier becomes negative, i.e. when

$$\mathbf{Q}\cdot\dot{\boldsymbol{\sigma}} \leqslant 0. \tag{13}$$

Reloading condition on crack flanks

Possibility of plastic reloading on crack flanks is allowed for by assuming [see Ponte Castañeda (1987a) and Östlund and Gudmundson (1988)] that reloading takes place when the stress state of the generic particle in the wake of the crack reaches the yield surface that was left at unloading. In other words, assuming a straight path motion of particles, the particle position at coordinate $\bar{x}_2$ is singled by its angular coordinate $\bar{\vartheta} = \tan^{-1}(\bar{x}_2/x_1)$ (Fig. 3). Therefore, by introducing the effective stress σ_e (defined in such a way that it reduces to the non-zero stress component in uniaxial tension):

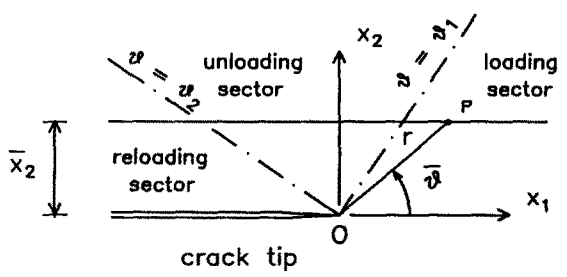

Fig. 3. Loading history of a generic material particle.

$$\sigma_e = \frac{3}{\mu+\sqrt{3}}\left[\frac{\mu}{3}\operatorname{tr}\boldsymbol{\sigma}+\sqrt{J_2}\right] = \underline{E}r^s y_e(\vartheta), \tag{14}$$

reloading takes place at the angle ϑ_2, if

$$y_e(\vartheta_1)/(\sin\vartheta_1)^s = y_e(\vartheta_2)/(\sin\vartheta_2)^s \quad \text{and} \quad \mathbf{Q}\cdot\dot{\boldsymbol{\sigma}} > 0, \tag{15}$$

where ϑ_1 is the angle corresponding to the elastic unloading and $y_e(\vartheta)$ is defined in agreement with (12). However, it is important to mention that (as in the J_2 plane stress case) reloading will be not revealed in the performed numerical analyses under plane stress conditions, whereas reloading will be found in plane strain.

Continuity conditions across the elastic–plastic boundaries

The continuity of displacements and velocities are requested across the elastic–plastic boundaries. Moreover, continuity of tractions implies:

$$[\![\sigma_{\vartheta\vartheta}]\!] = [\![\sigma_{r\vartheta}]\!] = 0, \tag{16}$$

where the symbol $[\![\ ]\!]$ stands for a jump in the relevant argument. However, the continuity of the radial stress and of the strain components is not trivial. As a matter of fact, it is proved that (Drugan and Rice, 1984; Drugan and Shen, 1990; Narasimhan and Rosakis, 1987; Nemat-Nasser and Gao, 1988), for quasi-static problems in elastoplasticity with (positive) isotropic hardening, all the stress components must be continuous if the material is stable in the Drucker sense. Thus, for the present model, full continuity of stress components must be imposed across the elastic–plastic boundaries.

3. PLANE STRESS

The plane stress conditions:

$$\sigma_{33} = \sigma_{13} = \sigma_{23} = 0 \tag{17}$$

make $\dot{\varepsilon}_{33}$ dependent on the non-zero components of $\dot{\boldsymbol{\sigma}}$. In fact, from (3), it is readily obtained:

$$\dot{\varepsilon}_{33} = \frac{1}{E}\left[-\nu(\dot{\sigma}_{rr}+\dot{\sigma}_{\vartheta\vartheta}) + \frac{1}{\hbar}\langle\mathbf{Q}\cdot\dot{\boldsymbol{\sigma}}\rangle Q_{33}\right]. \tag{18}$$

Equations (8) and (3), using (10_{1-3}) and (11), yield a system of five first order Partial Differential Equations (PDEs) in the five dependent variables v_r, v_ϑ, σ_{rr}, $\sigma_{\vartheta\vartheta}$ and $\sigma_{r\vartheta}$.

System of ODEs

The substitution of (12) into (8) and (3) yields a system of five first order Ordinary Differential Equations (ODEs) in the standard form:

$$\mathbf{y}' = \mathbf{f}(\mathbf{y}, \vartheta, s, \operatorname{sign}(f(\boldsymbol{\sigma})), \quad \operatorname{sign}(\mathbf{Q}\cdot\dot{\boldsymbol{\sigma}})). \tag{19}$$

It should be stressed that the form of system (19) depends on the condition of plastic loading, i.e. on $\operatorname{sign}(f(\boldsymbol{\sigma}))$ and $\operatorname{sign}(\mathbf{Q}\cdot\dot{\boldsymbol{\sigma}})$. In fact, unloading occurs when the plastic multiplier becomes negative whereas plastic reloading occurs when the yield function is reached again, i.e. when $f(\boldsymbol{\sigma})$ becomes zero.

The system (19) is written as:

$$y'_3 = y_5-(s+1)y_4, \tag{20a}$$

$$y'_5 = -(s+2)y_3, \tag{20b}$$

$$y'_4 = \frac{1}{\Delta}[y_1+(2-\nu s)\sin\vartheta\, y_3+s(y_4-\nu y_5)\cos\vartheta] + \frac{\langle\underline{\Lambda}\rangle}{\underline{\Lambda}}\frac{1}{\hbar\Delta}\left[\frac{\mu}{3}+\frac{2y_4-y_5}{6\sqrt{\underline{J}_2}}\right]\left[\Theta_1\sin\vartheta\, y_3+s\Theta_2\cos\vartheta\right], \tag{20c}$$

$$y'_1 = (1-s)y_2-2(1+\nu)s^2(\sin\vartheta\, y_4+\cos\vartheta\, y_3)+\frac{s}{\hbar\sqrt{\underline{J}_2}}\langle\underline{\Lambda}\rangle y_3, \tag{20d}$$

$$y'_2 = -y_1-s\sin\vartheta\,[\nu y'_4+(s-2\nu)y_3]+s^2\cos\vartheta\,(\nu y_4-y_5) + \frac{1}{\hbar}s\langle\underline{\Lambda}\rangle\left[\frac{\mu}{3}+\frac{2y_5-y_4}{6\sqrt{\underline{J}_2}}\right], \tag{20e}$$

where $1/\hbar = 0$ if $f(\sigma) < 0$ and:

$$\Delta = \sin\vartheta\left\{1+\frac{1}{\hbar}\left[\frac{\mu}{3}+\frac{2y_4-y_5}{6\sqrt{\underline{J}_2}}\right]^2\right\}, \tag{21}$$

which is always positive for $\hbar > 0$ and $\sin\vartheta \neq 0$,

$$\Theta_1 = (s+2)\frac{\mu}{3}+\frac{2(s-1)y_5+(5s+4)y_4}{6\sqrt{\underline{J}_2}}, \tag{22}$$

$$\Theta_2 = \frac{\mu}{3}(y_4+y_5)+\sqrt{\underline{J}_2}, \tag{23}$$

$$\underline{\Lambda} = y'_4\sin\vartheta\left[\frac{\mu}{3}+\frac{2y_4-y_5}{6\sqrt{\underline{J}_2}}\right]-y_3\Theta_1\sin\vartheta-s\Theta_2\cos\vartheta, \tag{24}$$

$$\underline{J}_2 = \tfrac{1}{3}(y_4^2+y_5^2-y_4y_5)+y_3^2. \tag{25}$$

It should be noted that eqns (20a) and (20b) are directly derived from the equilibrium eqns (8) and y'_4 has been explicitly solved by substituting (20a) and (20b) into the constitutive equation (3) corresponding to $\dot{\varepsilon}_{rr}$. Equations (20) reduce to the analogous equations given by Ponte Castañeda (1987a), when the parameter μ is set equal to zero.

Boundary conditions

The mode I symmetry and the regularity of the functions $\sigma_{\alpha\beta}$ ($\alpha, \beta = r, \vartheta$) ahead of the crack tip require:

$$v_\vartheta(0) = \sigma_{r\vartheta}(0) = \left(\frac{\partial\sigma_{rr}}{\partial\vartheta}\right)_{\vartheta=0} = 0, \tag{26}$$

i.e. in terms of functions y_i:

$$y_2(0) = y_3(0) = y'_4(0) = 0. \tag{27}$$

Moreover, on the crack surface, tensions $\sigma_{r\vartheta}$ and $\sigma_{\vartheta\vartheta}$ must vanish; hence:

$$y_3(\pi) = y_5(\pi) = 0. \tag{28}$$

Equations (27) and (28) represent five homogeneous independent boundary conditions. In addition to the previous five conditions, the following condition on $y_1(0)$ is obtained, by substituting eqns (27) into (20c):

$$y_1(0) = -s\left\{y_4(0) - \nu y_5(0) + \frac{1}{h}\left[\frac{\mu}{3} + \frac{2y_4(0) - y_5(0)}{2\sqrt{3[y_4^2(0) + y_5^2(0) - y_4(0)y_5(0)]}}\right]\right.$$
$$\left.\times\left[\frac{\mu}{3}[y_4(0) + y_5(0)] + \sqrt{[y_4^2(0) + y_5^2(0) - y_4(0)y_5(0)]/3}\right]\right\}. \tag{29}$$

Moreover, eqns (20) yield the following auxiliary equations:

$$y_1'(0) = y_5'(0) = 0, \tag{30}$$

$$y_3'(0) = y_5(0) - (1+s)y_4(0). \tag{31}$$

Finally, at elastic–plastic boundaries functions y_i cannot suffer jumps:

$$[\![y_1]\!] = [\![y_2]\!] = \cdots = [\![y_5]\!] = 0. \tag{32}$$

Integration of equations

The main advantage of the method of solution followed up to this point [analogous to that of Ponte Castañeda (1987a)] is that the system of ODEs can be solved by using the standard Runge–Kutta procedure. However, in order to start the integration, all the initial values of the functions y_i are required at point $\vartheta = 0$. Therefore, the normalization condition $y_4(0) = 1$ is used and the values of $y_5(0) = q$ and s are assigned tentatively. The integration is then performed and the values $y_3(\pi)$ and $y_5(\pi)$ are checked. On the basis of the error on $y_3(\pi)$ and $y_5(\pi)$, the initial values q and s are reassigned and the process is iterated. As in Östlund and Gudmundson (1988), the modified Powell hybrid method was used for the iteration on q and s. When the solution is obtained, all results are re-normalized assuming $y_e(\vartheta_1) = 1$. The numerical values reported in the next section, have been obtained by using standard double-precision routines, available in the IMSL library (subroutine DIVPRK for the Runge–Kutta method and subroutine DNEQNF for the Powell method).

Results

As in the case of the J_2-flow theory, variations in the values of ν have been found to have little influence on stress plots. Thus, all the following results are given in the case $\nu = 1/2$. Coherently with the plane stress J_2-flow theory, reloading was never revealed in all the numerical results. In Table 1 the values of the singularity s and of the unloading

Table 1. Values of s, q and ϑ_1 ($\nu = 1/2$)

$\alpha = 0.001$			
μ	s	q	ϑ_1
0.0	−0.02866	1.96890	53.202
0.2	−0.02656	2.45930	47.770
0.3	−0.02578	2.81838	45.502
0.4	−0.02515	3.31713	43.445
0.5	−0.02467	4.06674	41.559
0.6	−0.02430	5.33904	39.816
0.8	−0.02394	17.65462	36.692
$\alpha = 0.1$			
μ	s	q	ϑ_1
0.0	−0.23726	1.60583	73.646
0.2	−0.21810	1.92533	69.296
0.3	−0.21043	2.13341	67.468
0.4	−0.20379	2.39237	65.826
0.6	−0.19302	3.18331	63.016
0.8	−0.18497	4.92100	60.732
1.0	−0.17914	12.61329	58.894
1.1	−0.17694	101.54746	58.129

angle ϑ_1 (in degrees) are reported for $\alpha = 0.001$ and $\alpha = 0.1$. It should be noted that the values coincide with those of Ponte Castañeda (1987a) in the case of $\mu = 0$. The table shows a first effect of pressure-sensitivity, consisting of *a decrease (with increasing μ) of the amplitude of the plastic sector*. Moreover, parameters s and q increase with μ. In the following figures, the values of functions y_i ($-y_i$ for y_1 and y_2), evaluated for $y_e(\vartheta_1) = 1$, are reported. These values represent (except for an amplitude factor) the stress and velocity fields. These fields are reported in Figs 4 and 5 for the case of $\mu = 0.3$ and $\alpha = 0.001$. Plots of stress and velocity fields are reported in Figs 6–10 for $\alpha = 0.001$ and in Figs 11–15 for

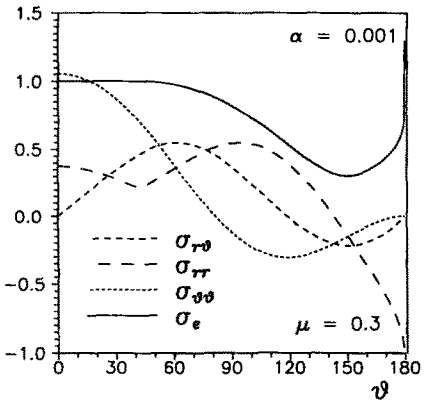

Fig. 4. Angular stress distribution for small strain hardening (plane stress).

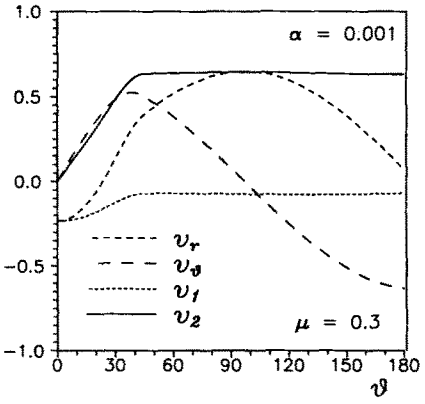

Fig. 5. Angular velocities distribution for small strain hardening in Cartesian and cylindrical components (plane stress).

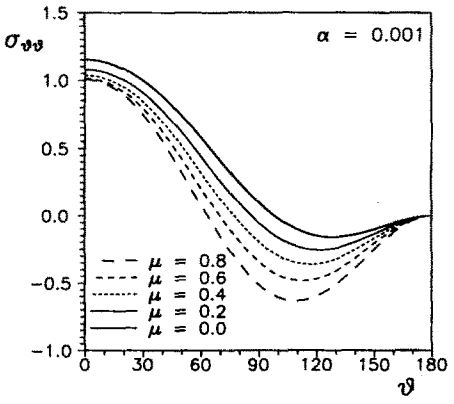

Fig. 6. Angular distribution of hoop stresses for small strain hardening and various degrees of pressure-sensitivity (plane stress).

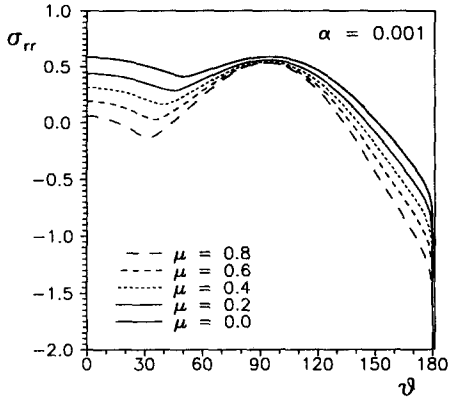

Fig. 7. Angular distribution of radial stresses for small strain hardening and various degrees of pressure-sensitivity (plane stress).

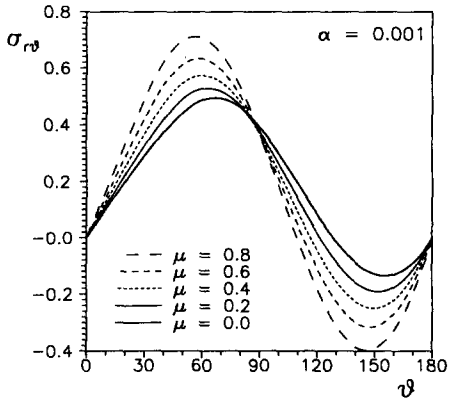

Fig. 8. Angular distribution of shear stresses for small strain hardening and various degrees of pressure-sensitivity (plane stress).

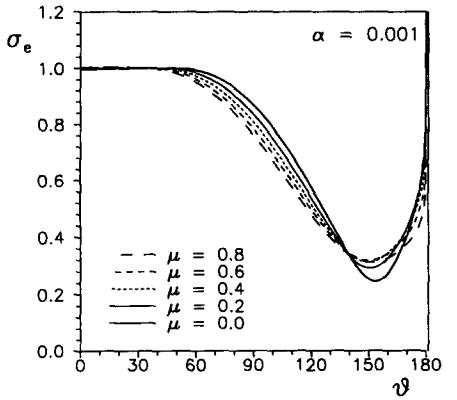

Fig. 9. Angular distribution of effective stress for small strain hardening and various degrees of pressure-sensitivity (plane stress).

$\alpha = 0.1$. The cases of $\mu = 0$–0.8 are considered. It can be noted that the effects caused by the pressure-sensitivity decrease for high values of α where all the fields tend to approach the elastic solution. The main differences with respect to the J_2-flow theory, become evident for low values of α and can be summarized as:

—a reduction is observed in the amplitude of the plastic sector;
—a reduction is observed in the radial stress ahead of the crack tip;

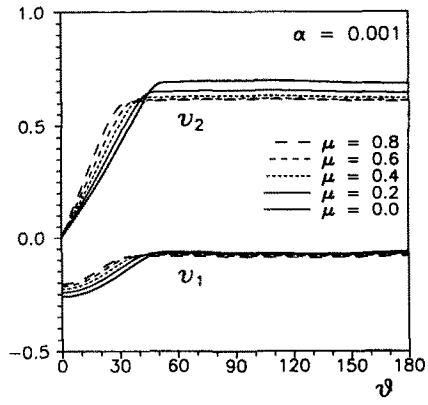

Fig. 10. Angular distribution of velocities in Cartesian coordinates for small strain hardening and various degrees of pressure-sensitivity (plane stress).

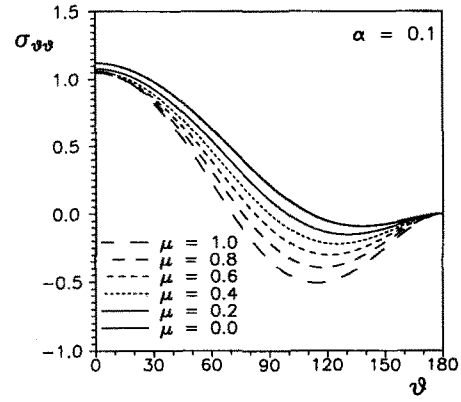

Fig. 11. Angular distribution of hoop stresses for high strain hardening and various degrees of pressure-sensitivity (plane stress).

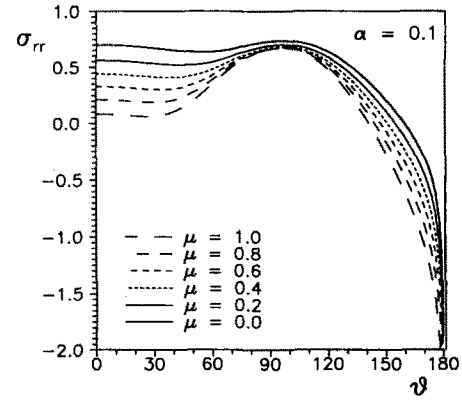

Fig. 12. Angular distribution of radial stresses for high strain hardening and various degrees of pressure-sensitivity (plane stress).

—a corresponding reduction is observed in the mean normal stress ahead of the crack tip.

All effects become more evident by increasing μ and decreasing α. The last two conclusions are in good agreement with the observations of Li and Pan (1990b). In the perfect-plasticity case, these authors found a decrease in $\sigma_{rr}(0)$ with μ, until an asymptote for q is reached ($\sigma_{rr}(0) \to 0$, for $\mu = \sqrt{3}/2$). For small values of α, an analogous behavior

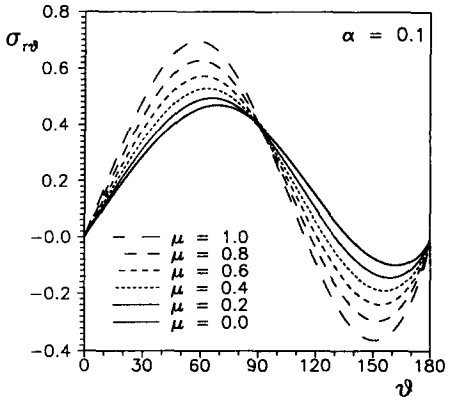

Fig. 13. Angular distribution of shear stresses for high strain hardening and various degrees of pressure-sensitivity (plane stress).

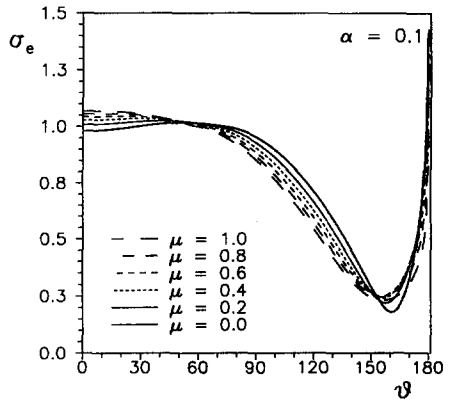

Fig. 14. Angular distribution of effective stress for high strain hardening and various degrees of pressure-sensitivity (plane stress).

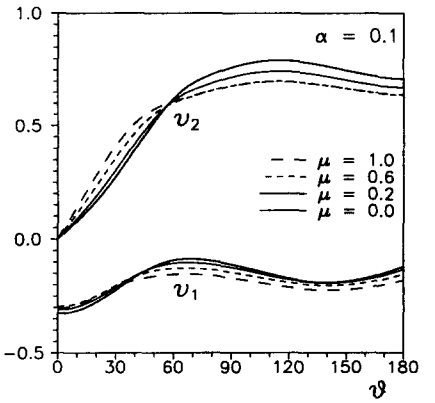

Fig. 15. Angular distribution of velocities in Cartesian coordinates for high strain hardening and various degrees of pressure-sensitivity (plane stress).

is observed using the present model (see Table 2). However, for high values of hardening, $\sigma_{rr}(0)$ tends to vanish when μ approaches values greater than $\sqrt{3}/2$ (see Table 1).

4. PLANE STRAIN

The plane strain condition

$$\dot{\varepsilon}_{33} = 0, \tag{33}$$

together with (11) and (10) can be substituted into the constitutive equations (3) and into

Table 2. Values of s, q and ϑ_1 near the asymptote of q

$\alpha = 0.001$, $\nu = 1/2$			
μ	s	q	ϑ_1
0.82	−0.02393	23.66994	36.404
0.84	−0.02393	36.29621	36.120
0.86	−0.02393	79.78314	35.840
0.87	−0.02393	204.12636	35.800

the equilibrium equations (8). In this way a system of six first order PDEs can be obtained in the six unknown functions σ_{rr}, $\sigma_{\vartheta\vartheta}$, $\sigma_{r\vartheta}$, σ_{33}, v_r, v_ϑ. Solutions of this system are sought in the HHR form (12).

System of ODEs

The substitution of (12) into (8) and (3) yields a system of six ODEs in the standard form (19), which can be expanded as:

$$y_3' = y_5 - (s+1)y_4, \tag{34a}$$

$$y_5' = -(s+2)y_3, \tag{34b}$$

$$y_4' = sy_4 \cot\vartheta + 2y_3 + \frac{1}{\sin\vartheta}\dot{\underline{\sigma}}_{rr}, \tag{34c}$$

$$y_6' = \frac{1}{\sin\vartheta}[sy_6 \cos\vartheta + \dot{\underline{\sigma}}_{33}], \tag{34d}$$

$$y_2' = -y_1 + s[\dot{\underline{\sigma}}_{\vartheta\vartheta} - \nu(\dot{\underline{\sigma}}_{rr} + \dot{\underline{\sigma}}_{33}) + \underline{\Lambda} Q_{\vartheta\vartheta}], \tag{34e}$$

$$y_1' = (1-s)y_2 + 2s[(1+\nu)\dot{\underline{\sigma}}_{r\vartheta} + \underline{\Lambda} Q_{r\vartheta}], \tag{34f}$$

where

$$\dot{\underline{\sigma}}_{ij} = \frac{\dot{\sigma}_{ij}}{\sqrt{E} r^{s-1}}, \tag{35}$$

$$\dot{\underline{\sigma}}_{\vartheta\vartheta} = -s(y_3 \sin\vartheta + y_5 \cos\vartheta), \tag{36}$$

$$\dot{\underline{\sigma}}_{r\vartheta} = -s(y_4 \sin\vartheta + y_3 \cos\vartheta), \tag{37}$$

$$\dot{\underline{\sigma}}_{rr} = \frac{1}{\Delta}\{\dot{\underline{\sigma}}_{\vartheta\vartheta}[\nu(1+\nu)k + \nu Q_{33}(Q_{33} - Q_{\vartheta\vartheta}) - Q_{rr}(Q_{\vartheta\vartheta} + \nu Q_{33})] - 2\dot{\underline{\sigma}}_{r\vartheta} Q_{r\vartheta}(Q_{rr} + \nu Q_{33}) + y_1(k + Q_{33}^2)\}, \tag{38}$$

$$\dot{\underline{\sigma}}_{33} = \frac{1}{k + Q_{33}^2}[\nu k(\dot{\underline{\sigma}}_{rr} + \dot{\underline{\sigma}}_{\vartheta\vartheta}) - Q_{33}(Q_{rr}\dot{\underline{\sigma}}_{rr} + Q_{\vartheta\vartheta}\dot{\underline{\sigma}}_{\vartheta\vartheta} + 2Q_{r\vartheta}\dot{\underline{\sigma}}_{r\vartheta})], \tag{39}$$

$$Q_{rr} = \frac{\mu}{3} + \frac{2y_4 - y_5 - y_6}{6\sqrt{J_2}}, \quad Q_{\vartheta\vartheta} = \frac{\mu}{3} + \frac{2y_5 - y_4 - y_6}{6\sqrt{J_2}},$$

$$Q_{r\vartheta} = \frac{y_3}{2\sqrt{J_2}}, \quad Q_{33} = \frac{\mu}{3} + \frac{2y_6 - y_5 - y_4}{6\sqrt{J_2}}, \tag{40}$$

$$\Delta = (1-\nu^2)\hbar + (Q_{33}^2 + Q_{rr}^2 + 2\nu Q_{rr}Q_{33}), \tag{41}$$

which is always positive for $\hbar > 0$, and

$$\underline{\Lambda} = \frac{1}{\hbar}[Q_{rr}\underline{\dot{\sigma}}_{rr} + Q_{\vartheta\vartheta}\underline{\dot{\sigma}}_{\vartheta\vartheta} + Q_{33}\underline{\dot{\sigma}}_{33} + 2Q_{r\vartheta}\underline{\dot{\sigma}}_{r\vartheta}], \tag{42}$$

$$\underline{J}_2 = \tfrac{1}{3}(y_4^2 + y_5^2 + y_6^2 - y_4y_5 - y_5y_6 - y_4y_6) + y_3^2. \tag{43}$$

When $f(\boldsymbol{\sigma}) < 0$, the elastic solution can be obtained from (34)–(43) by taking the limit $\hbar \to +\infty$. It is worth noting that (34a,b) can be obtained by substituting (12) into (8). A substitution of (12) and (34a,b) into (10_1) and (10_3) yields (36) and (37). Moreover (38) and (39) can be obtained using the plane strain condition $\dot{\varepsilon}_{33} = 0$, (11) and (12) in the constitutive equations (3) that give $\dot{\varepsilon}_{rr}$ and $\dot{\varepsilon}_{33}$. Equations (34c,d) follow from a substitution of (12) into (10_2) and (10_4). Finally, (43) and (11), using (3), give (34e,f).

Boundary conditions

Mode I symmetry and the regularity of functions y_i in $\vartheta = 0$ requires:

$$y_2(0) = y_3(0) = y_4'(0) = y_5'(0) = y_6'(0) = 0, \tag{44}$$

while the vanishing of $\sigma_{r\vartheta}$ and $\sigma_{\vartheta\vartheta}$ on the crack surface requires:

$$y_3(\pi) = y_5(\pi) = 0. \tag{45}$$

It should be noted that only four of the conditions (44) are independent, in fact (44_4) can be obtained from the others by using (34b). In addition to (44), the following auxiliary boundary conditions can be obtained from (34e) and (33), taking into account (44):

$$y_1(0) = -s\left\{y_4(0) - \nu[y_5(0) + y_6(0)] + \frac{1}{\hbar}\left[\frac{\mu}{3} + \frac{2y_4(0) - y_5(0) - y_6(0)}{6\sqrt{\underline{J}_2(0)}}\right] \times \left[\frac{\mu}{3}(y_4(0) + y_5(0) + y_6(0)) + \sqrt{\underline{J}_2(0)}\right]\right\}, \tag{46}$$

$$y_6(0) - \nu[y_5(0) + y_4(0)] + \frac{1}{\hbar}\left[\frac{\mu}{3} + \frac{2y_6(0) - y_5(0) - y_4(0)}{6\sqrt{\underline{J}_2(0)}}\right] \times \left[\frac{\mu}{3}(y_4(0) + y_5(0) + y_6(0)) + \sqrt{\underline{J}_2(0)}\right] = 0. \tag{47}$$

Continuity of all fields across elastic–plastic boundaries requires:

$$[\![y_1]\!] = [\![y_2]\!] = \cdots = [\![y_6]\!] = 0. \tag{48}$$

Integration of equations

Similarly to the plane stress case, (34) is solved with the Runge–Kutta method, starting with the normalization $y_5(0) = 1$ and two tentative values of s and $y_4(0) = q$. Differently from the plane stress case, $y_6(0)$ is obtained solving (47) with a non-linear equation solver (subroutine DZBREN in the IMSL library). When s and q are obtained, the results are re-normalized assuming $y_e(\vartheta_1) = 1$.

Table 3. Values of s, q, ϑ_1 and ϑ_2 ($\nu = 1/3$)

μ	s	q	ϑ_1	ϑ_2
		$\alpha = 0.75$		
0.00	−0.48063	1.11817	91.524	~180.000
0.10	−0.47536	1.09930	88.999	180.000
0.20	−0.46948	1.07705	86.784	180.000
0.30	−0.46315	1.05311	84.833	180.000
0.40	−0.45654	1.03045	83.099	180.000
0.50	−0.44980	1.00990	81.555	180.000
		$\alpha = 0.1$		
μ	s	q	ϑ_1	ϑ_2
0.00	−0.20956	1.09031	122.012	175.318
0.10	−0.20186	1.01006	107.416	179.845
		$\alpha = 0.01$		
μ	s	q	ϑ_1	ϑ_2
0.00	−0.08242	0.79740	134.998	146.242
0.10	−0.07840	0.88486	131.477	144.584
0.20	−0.07415	0.99017	127.663	143.727
		$\alpha = 0.001$		
μ	s	q	ϑ_1	ϑ_2
0.00	−0.05640	0.75379	136.965	138.444
0.10	−0.05367	0.82806	133.816	135.458
0.20	−0.05002	0.89693	130.549	132.531
0.30	−0.04561	0.96363	127.095	129.741
0.33	−0.04405	0.98837	125.999	128.962
		$\alpha = 0.0001$		
μ	s	q	ϑ_1	ϑ_2
0.00	−0.05360	0.75007	137.421	137.916
0.10	−0.05094	0.82305	134.293	134.772
0.20	−0.04709	0.88960	131.060	131.519
0.30	−0.04221	0.95054	127.671	128.105
0.33	−0.04055	0.96883	126.613	127.041
0.35	−0.03937	0.98229	125.894	126.319

Results

Values of the singularity s, of the parameter q and of the unloading and reloading angles ϑ_1 and ϑ_2 are reported in Table 3, in the cases $\nu = 1/3$, $\alpha = 0.0001$–0.75, for various values of μ. For the same values of parameters, the plots of stress and velocity components are reported in Figs (16)–(27). In contrast to the plane stress case, the plots of the stress components are reported in the same figure for given values of μ. In this way, it becomes

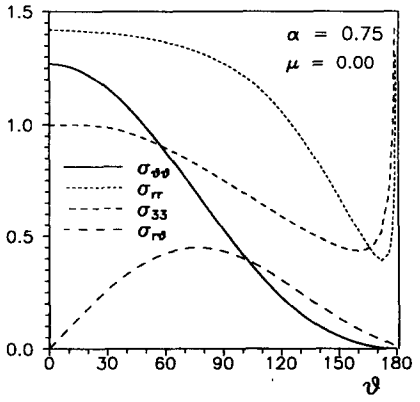

Fig. 16. Angular distribution of stress components for $\mu = 0$ and $\alpha = 0.75$ (plane strain).

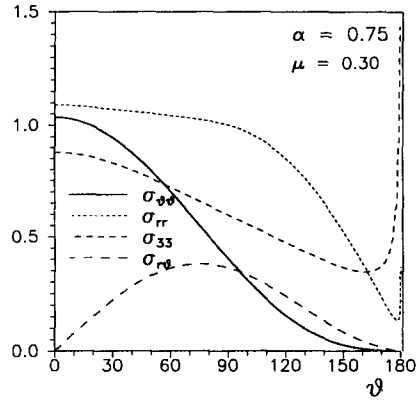

Fig. 17. Angular distribution of stress components for $\mu = 0.30$ and $\alpha = 0.75$ (plane strain).

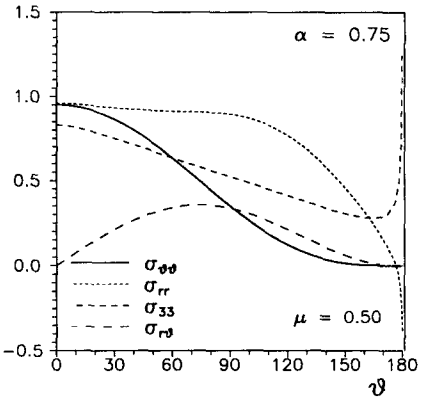

Fig. 18. Angular distribution of stress components for $\mu = 0.50$ and $\alpha = 0.75$ (plane strain).

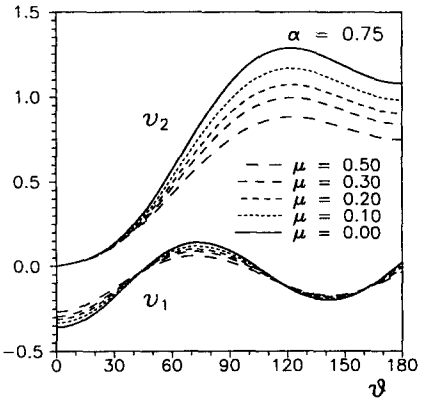

Fig. 19. Angular distribution of velocities in Cartesian coordinates for various degrees of pressure-sensitivity and $\alpha = 0.75$ (plane strain).

easier to estimate the tendency of the stress ahead of the tip to approach the hydrostatic state. It should be remarked that the value corresponding to $\mu = 0$ does not coincide with that of Ponte Castañeda (1987a) because of the different definition of α. As in plane stress, the effect of the pressure-sensitivity consists of a decrease in the stress singularity s and of the angle of unloading. Moreover, the reloading angle slightly decreases by increasing μ. It can also be noted that the pressure-sensitivity flattens the peak of the angular distribution of radial stress and translates it toward $\vartheta = 0$.

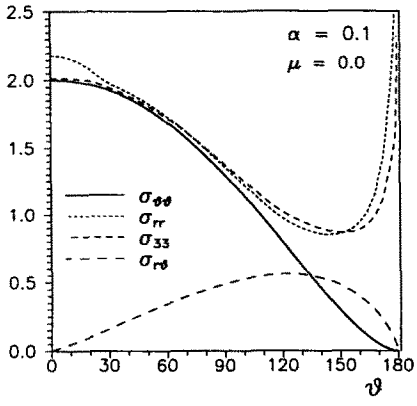

Fig. 20. Angular distribution of stress components for $\mu = 0$ and $\alpha = 0.10$ (plane strain).

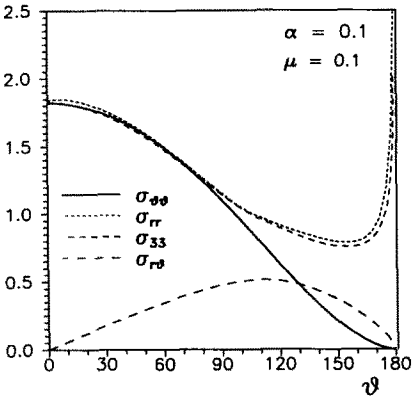

Fig. 21. Angular distribution of stress components for $\mu = 0.10$ and $\alpha = 0.10$ (plane strain).

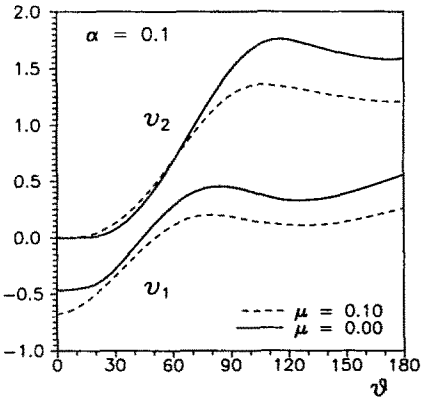

Fig. 22. Angular distribution of velocities in Cartesian coordinates for various degrees of pressure-sensitivity and $\alpha = 0.10$ (plane strain).

By increasing the pressure-sensitivity, the state of stress near $\vartheta = 0$ tends to a hydrostatic state of tension. This last observation is in agreement with the findings of Li and Pan (1990a) and, for a different pressure-sensitive model, of Hutchinson (1982). Therefore, by increasing the pressure-sensitivity, the stress point in the Haigh–Westergaard space, representative of the stress state ahead of the crack tip, tends to the vertex of the yield locus. At the vertex of the Drucker–Prager yield surface, the model has a singular behavior and the whole solution procedure should be re-formulated. As noted by Li and Pan (1990b), for any given value of hardening, a limit value μ_{lim} of pressure-sensitivity exists, for which

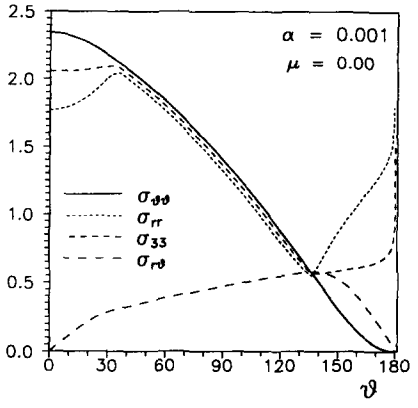

Fig. 23. Angular distribution of stress components for $\mu = 0$ and $\alpha = 0.001$ (plane strain).

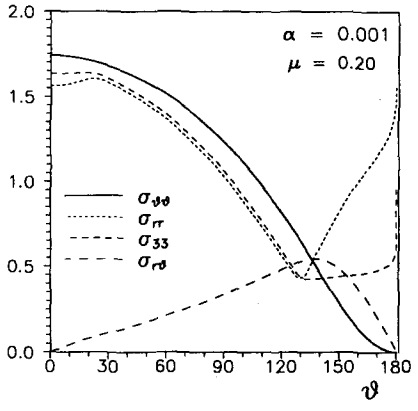

Fig. 24. Angular distribution of stress components for $\mu = 0.20$ and $\alpha = 0.001$ (plane strain).

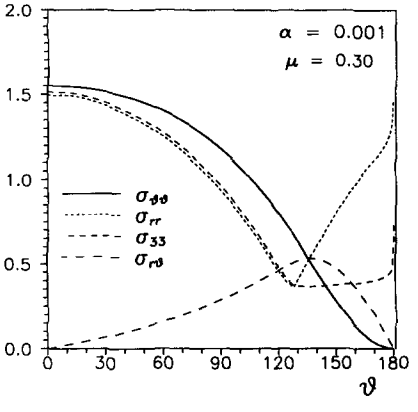

Fig. 25. Angular distribution of stress components for $\mu = 0.30$ and $\alpha = 0.001$ (plane strain).

the hydrostatic state of stress is reached at $\vartheta = 0$. However, Li and Pan (1990b) showed that μ_{lim} *increases* approaching the perfectly-plastic solution. The model of Li and Pan concerns the static problem and the hardening is not assumed to be constant. Therefore, a comparison between our model and that of Li and Pan is not straightforward. However, our results show a more involved trend (see Table 3). In fact, for high values of hardening, μ_{lim} increases by increasing the hardening and, vice versa, for low values of hardening μ_{lim} increases by decreasing the hardening.

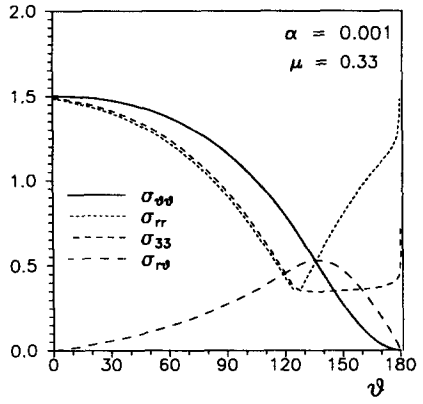

Fig. 26. Angular distribution of stress components for $\mu = 0.33$ and $\alpha = 0.001$ (plane strain).

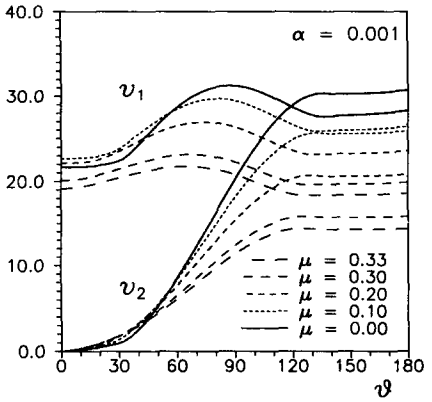

Fig. 27. Angular distribution of velocities in Cartesian coordinates for various degrees of pressure-sensitivity and $\alpha = 0.001$ (plane strain).

5. CONCLUSIONS

In this paper, the near tip fields of a steadily propagating crack under the mode I condition have been obtained for the Drucker–Prager incremental elastoplastic model.

From the present study it can be concluded that an increase in the pressure-sensitivity in the plane stress case produces:

—a reduction in the singularity of the fields;
—a reduction in the ratio between the radial and the hoop stresses ahead of the crack tip, connected with a decrease in the mean normal stress ahead of the crack tip;
—a reduction in size of the plastic sector;
—a sharpening of the peaks of the angular distributions of stress components.

The first observation is common with the plane strain case where, in addition, an increase in the pressure-sensitivity yields:

—a translation of the maximum in the radial stress toward the crack tip;
—a decrease in the stress deviator ahead of the crack tip.

It can be concluded that the pressure-sensitivity of the analysed model makes the singularity of the fields weaker than in the J_2-flow theory. This fact should imply a crack growth stabilization. An analogous stabilizing effect should also come from the observed relaxation in the stress ahead of the crack tip.

Acknowledgements—A grateful acknowledgement is due to the (Italian) Ministry of University and Scientific and Technological Research (MURST) and to the National Council of Research (CNR).

REFERENCES

Achenbach, J. D., Kanninien, M. F. and Popelar, C. H. (1981). Crack tip fields for fast fracture of an elastic–plastic material. *J. Mech. Phys. Solids* **29,** 211–225.

Amazigo, J. and Hutchinson, J. W. (1977). Crack-tip fields in steady crack-growth with linear strain hardening. *J. Mech. Phys. Solids* **25,** 81–97.

Aoki, S., Kishimoto, K., Takeya, A. and Sakata, M. (1984). Effects of microvoids on crack blunting and initiation in ductile materials. *Int. J. Fracture* **24,** 267–278.

Aoki, S., Kishimoto, K., Yoshida, T. and Sakata, M. (1987). A finite element study of the near crack tip deformation of a ductile material under mixed mode loading. *J. Mech. Phys. Solids* **35,** 431–455.

Budiansky, B. (1959). A reassessment of deformation theories of plasticity. *J. Appl. Mech.* 259–264.

Carapellucci, L. M. and Yee, A. F. (1986). The biaxial deformation and yield behavior of bisphenol—A polycarbonate: effect of anisotropy. *Polymer Engng Sci.* **26,** 920–930.

Chen, I. W. and Reyes-Morel, P. E. (1986). Implications of transformation plasticity in ZrO_2-containing ceramics: I, shear and dilatation effects. *J. Am. Ceram. Soc.* **69,** 181–189.

Drucker, D. C. (1973). Plasticity theory, strength-differential (SD) phenomenon, and volume expansion in metals and plastics. *Metall. Trans.* **4,** 667–673.

Drucker, D. C. and Prager, W. (1952). Soil mechanics and plastic analysis or limit design. *Q. Appl. Math.* **10,** 157–165.

Drugan, W. J. and Rice, J. R. (1984). Restrictions on quasi-statically moving surfaces of strong discontinuity in elastic–plastic solids. In *Mechanics of Material Behavior* (Edited by G. J. Dvorak and R. T. Shield), pp. 59–73. Elsevier, Amsterdam.

Drugan, W. J., Rice, J. R. and Sham, T. L. (1982). Asymptotic analysis of growing plane strain tensile cracks in elastic–ideally plastic solids. *J. Mech. Phys. Solids* **30,** 447–473.

Drugan, W. J. and Shen, Y. (1990). Finite deformation analysis of restrictions on moving strong discontinuity surfaces in elastic–plastic materials: quasi-static and dynamic deformations. *J. Mech. Phys. Solids* **38,** 553–574.

Evans, B. and Wong, T. F. (1985). Shear localization in rocks induced by tectonic deformation. In *Mechanics of Geomaterials* (Edited by Z. P. Bazant), pp. 189–210. Wiley, New York.

Gao, Y. C. (1987). Plane stress dynamic plastic field near a propagating crack tip. *Int. J. Fracture* **34,** 111–129.

Gupta, Y. M. (1977). Pressure-dependent yield and plastic volume change in high strength steels. *Acta Metall.* **25,** 1509–1513.

Gurson, A. L. (1977). Porous rigid-plastic materials containing rigid inclusions-yield function, plastic potential and void nucleation. In *Fracture* (Edited by D. M. R. Taplin), Vol. 2, pp. 357–364. University of Waterloo Press.

Hutchinson, J. W. (1968a). Singular behaviour at the end of a tensile crack in a hardening material. *J. Mech. Phys. Solids* **16,** 13–81.

Hutchinson, J. W. (1968b). Plastic stress and strain fields at a crack tip. *J. Mech. Phys. Solids* **16,** 337–347.

Hutchinson, J. W. (1982). Constitutive behavior and crack tip fields for materials undergoing creep-constrained grain boundary cavitation. *Acta Metall.* **31,** 1079–1088.

Kotsovos, M. D. and Newman, J. B. (1978). Generalized stress–strain relations for concrete. *J. Engng Mech. Div. ASCE* **104,** 845–856.

Li, F. Z. (1992). The analytic solution of near tip stress fields for perfectly plastic pressure-sensitive material under plane stress condition. *Int. J. Fracture* **53,** 325–336.

Li, F. Z. and Pan, J. (1990a). Plane-strain crack-tip fields for pressure-sensitive dilatant materials. *J. Appl. Mech.* **57,** 40–49.

Li, F. Z. and Pan, J. (1990b). Plane-stress crack-tip fields for pressure-sensitive dilatant materials. *Engr Fracture Mech.* **35,** 1105–1116.

Narasimhan, R. and Rosakis, A. J. (1987). Reexamination of jumps across quasi-statically propagating surfaces under generalized plane stress in anisotropically hardening elastic–plastic solids. *J. Appl. Mech.* **54,** 519–524.

Needleman, A. and Rice, J. R. (1978). Limits to ductility set by plastic flow localization. In *Mechanics of Sheet Metal Forming* (Edited by D. P. Koistinien and N. M. Wang), pp. 237–267. Plenum Press, New York.

Needleman, A. and Tvergaard, V. (1987). An analysis of ductile rupture modes at a crack. *J. Mech. Phys. Solids* **35,** 151–183.

Needleman, A. and Tvergaard, V. (1992). Effect of crack meandering on dynamic, ductile fracture. *J. Mech. Phys. Solids* **40,** 447–471.

Nemat-Nasser, S. and Gao, Y. C. (1988). Discontinuities in elastic–plastic solids. *Mech. Materials* **7,** 215–229.

Östlund, S. and Gudmundson, P. (1988). Asymptotic crack tip fields for dynamic fracture of linear strain-hardening solids. *Int. J. Solids Structures* **24,** 1141–1148.

Ponte Castañeda, P. (1987a). Asymptotic fields in steady crack growth with linear strain-hardening. *J. Mech. Phys. Solids* **35,** 227–268.

Ponte Castañeda, P. (1987b). Plastic stress intensity factors in steady crack growth. *J. Appl. Mech.* **54,** 379–387.

Radi, E. and Bigoni, D. (1993). Asymptotic fields of mode I steady-state crack propagation in non-associative elastoplastic solids. *Mech. Mater.* (in press).

Reyes-Morel, P. E. and Chen, I. W. (1988). Transformation plasticity of CeO_2-stabilized tetragonal zirconia polycrystals: I, stress assistance and autocatalysis. *J. Am. Ceram. Soc.* **71,** 343–353.

Rice, J. R. (1982). Elastic–plastic crack growth. In *Mechanics of Solids: The Rodney Hill 60th Anniversary Volume* (Edited by H. G. Hopkins and M. J. Sewell), pp. 539–562. Pergamon Press, Oxford.

Rice, J. R., Drugan, W. J. and Sham, T. L. (1980). Elastic–plastic analysis of growing cracks. *Fracture Mech.* **ASTM-STP 700,** 189–219.

Rice, J. R. and Rosengren, G. F. (1968). Plane strain deformation near a crack tip in a power-law hardening material. *J. Mech. Phys. Solids* **10,** 1–12.

Rudnicki, J. W. (1977). The inception of faulting in a rock mass with a weakened zone. *J. Geophys. Res.* **82,** 844–854.

Slepyan, L. I. (1974). Growing crack during plane deformation of an elastic plastic body. *Mekhanika Tverdogo Tela* **9**, 57–67.
Spitzig, W. A. and Richmond, O. (1979). Effect of hydrostatic pressure on the deformation behavior of polyethylene and polycarbonate in tension and in compression. *Polim. Engng Sci.* **19**, 1129–1139.
Spitzig, W. A., Sober, R. J. and Richmond, O. (1975). Pressure dependence of yielding and associated volume expansion in tempered martensite. *Acta Metall.* **23**, 885–893.
Spitzig, W. A., Sober, R. J. and Richmond, O. (1976). The effect of hydrostatic pressure on the deformation behavior of maraging and HY-80 steels and its implications for plasticity theory. *Metall. Trans.* **7A**, 1703–1710.
Whitney, W. and Andrews, R. D. (1967). Yielding of glassy polymer: volume effects. *J. Polim. Sci.* **16**, 2981–2990.

APPENDIX

Derivation of eqns (21)

Let $\mathbf{e}_1$ and $\mathbf{e}_2$ be the unit vectors in the directions x_1 and x_2 respectively, $\mathbf{e}_r$ the unit vector in the r direction and $\mathbf{e}_\vartheta$ the unit vector orthogonal to $\mathbf{e}_r$ (in the plane of $\mathbf{e}_1$ and $\mathbf{e}_2$). The material derivative of the component $\sigma_{r\vartheta}$ is defined as:

$$(\mathbf{e}_r \cdot \boldsymbol{\sigma}\mathbf{e}_\vartheta)^{\cdot} = \mathbf{e}_r \cdot \dot{\boldsymbol{\sigma}}\mathbf{e}_\vartheta + \dot{\mathbf{e}}_r \cdot \boldsymbol{\sigma}\mathbf{e}_\vartheta + \mathbf{e}_r \cdot \boldsymbol{\sigma}\dot{\mathbf{e}}_\vartheta. \tag{A1}$$

By performing the material derivative of the following coordinate transformations:

$$\begin{cases} \mathbf{e}_r = \cos\vartheta\,\mathbf{e}_1 + \sin\vartheta\,\mathbf{e}_2, \\ \mathbf{e}_\vartheta = -\sin\vartheta\,\mathbf{e}_1 + \cos\vartheta\,\mathbf{e}_2, \end{cases} \tag{A2}$$

the following is obtained:

$$\begin{cases} \dot{\mathbf{e}}_r = (\cos\vartheta)^{\cdot}\mathbf{e}_1 + (\sin\vartheta)^{\cdot}\mathbf{e}_2, \\ \dot{\mathbf{e}}_\vartheta = -(\sin\vartheta)^{\cdot}\mathbf{e}_1 + (\cos\vartheta)^{\cdot}\mathbf{e}_2. \end{cases} \tag{A3}$$

From (A3), using (6) and (9a) the following is readily obtained:

$$\begin{cases} \dot{\mathbf{e}}_r = \mathscr{V}\frac{1}{r}\sin\vartheta\,\mathbf{e}_\vartheta, \\ \dot{\mathbf{e}}_\vartheta = -\mathscr{V}\frac{1}{r}\sin\vartheta\,\mathbf{e}_r. \end{cases} \tag{A4}$$

Using (A4), (A1) gives:

$$\mathbf{e}_r \cdot \dot{\boldsymbol{\sigma}}\mathbf{e}_\vartheta = (\mathbf{e}_r \cdot \boldsymbol{\sigma}\mathbf{e}_\vartheta)^{\cdot} - \mathscr{V}\frac{\sin\vartheta}{r}(\mathbf{e}_\vartheta \cdot \boldsymbol{\sigma}\mathbf{e}_\vartheta - \mathbf{e}_r \cdot \boldsymbol{\sigma}\mathbf{e}_r). \tag{A5}$$

The derivative of the component $\sigma_{r\vartheta}$ in eqn (A5) can be transformed via (6) and (9a). In this way eqn (10a) is obtained. Equations (10b) and (10c) can be obtained with a procedure analogous to the above if the substitutions $\mathbf{e}_\vartheta \to \mathbf{e}_r$ and $\mathbf{e}_r \to \mathbf{e}_\vartheta$ are made.